ISSN 0010-9525, Cosmic Research, 2019, Vol. 57, No. 6, pp. 389–406. © Pleiades Publishing, Ltd., 2019.
Russian Text © The Author(s), 2019, published in Kosmicheskie Issledovaniya, 2019, Vol. 57, No. 6, pp. 403–422.

Physical Mechanism of a Solar Flare Based on the Accumulation of the Energy in the Magnetic Field of the Current Sheet in the Solar Corona

I. M. Podgorny[a, †] and A. I. Podgorny[b, *]

[a] *Institute of Astronomy, Russian Academy of Sciences, Moscow, 119017 Russia*
[b] *Lebedev Physical Institute, Russian Academy of Sciences, Moscow, 119991 Russia*
**e-mail: podgornyjai@lebedev.ru*

Received April 16, 2019; revised April 22, 2019; accepted April 25, 2019

Abstract—During a solar flare, the magnetic energy of ~10^{32} erg is released in a few dozens of minutes. The invariability of the magnetic field on the solar surface during flares proves the appearance of a flare in the corona. An analysis of the dynamics of the electron temperature of the solar atmosphere provides independent evidence of the coronal origin of the flare. The appearance of the flare in the corona is explained by the release of the energy accumulated in the magnetic field of the current sheet. To study the flare situation, numerical MHD simulation was performed for a real active region. The simulation results showed the appearance of a current sheet, which position coincides with the position of the observed source of thermal X-ray emission. A methodology for calculations in real time scale has been developed. Based on the mechanism of energy release in the current sheet, an electrodynamic model of a solar flare is proposed, which explains its main observed manifestations. Sources of hard X-ray emission appear due to deceleration in the lower dense layers of the solar atmosphere of electron beams accelerated in field-aligned currents. The acceleration of solar cosmic rays occurs in the current sheet by the electric field $\mathbf{E} = -\mathbf{V} \times \mathbf{B}/c$, and not in shock waves.

DOI: 10.1134/S0010952519060054

1. INTRODUCTION

During a solar flare, ~10^{32} erg of magnetic energy is released in a few dozens of minutes, which transforms into the energy of heated plasma (at the place of the flare in the solar corona, the temperature rises to 30–50 MK (million degrees K) compared to ~1 MK background corona), the kinetic energy of plasma ejections into the interplanetary medium (their mass reaches ~10^{14} g, and the velocity is ~10^7 cm/s), the energy of accelerated charged particles (solar cosmic rays, mainly protons with the energy up to 20 GeV), and the emission energy in the wide range: radio, optical, UV emissions, X-ray emission (soft thermal 1–20, hard beam 20–200, and higher keV) generated by accelerated electrons and thermal electrons of heated plasma, as well as and γ-ray emission resulting from nuclear reactions under the action of accelerated protons incident in the Sun. The most interesting and unusual phenomenon that occurs during solar flares is the acceleration of charged particles up to energies significantly higher than the thermal (the appearance of solar cosmic rays). During the flare, the magnetic energy is released, because flares occur above the active region with the large magnetic field (on the solar surface, it reaches 3000 Gs). The unique reservoir of the energy needed for a flare (~10^{32} erg) in the corona can be the magnetic field, where the field energy $B^2/8\pi$ significantly exceeds the thermal energy of plasma nkT.

The primordial release of solar flare energy occurs in the solar corona at the altitudes of 15000–30000 km, which is proved experimentally by observations with high resolution of thermal X-ray emission from flares at the limb [1]. There is a number of other observational evidence of the energy release of the flare in the corona. Observations of the preflare situation and the flare in the spectral lines of highly ionized iron ions (emitting at the temperature of 6.3, 10, and 20 MK) show the evolution before the flare of a structure with the high temperature, which can appear only in the hot corona, and a sharp increase in the temperature in this structure during the flare. Flare energy release in the corona is clearly observed in the lines of iron ions for flares at the disk limb. During the flare, there is no significant variation in the magnetic field on the solar surface, while significant variations in the field on the surface would have to occur during flare energy release in the chromosphere or the photosphere. Observations of the manifestations of flares in the photosphere (H_α 6563 Å line in the photo-

† Deceased.

sphere, 1600 Å line of the CIV ion in the transition region between the chromosphere and the corona) always show the appearance of at least two ribbons, which is explained by the propagation of fast electrons from the flare point into the chromosphere along magnetic lines emerging from the current sheet. If the flare energy were released in the chromosphere, the appearance of only one bright region would be most realistic, at least, in some flares.

Understanding the mechanism of a solar flare, which makes it possible, using numerical MHD simulation, to establish the flare situation in the solar corona and to find the place of accumulation of the magnetic energy for the solar flare, can improve the quality of the forecast of solar flares. At present, phenomenological features are used to forecast solar flares without understanding the physical mechanism of the flare. However, some precursors that, as experience has shown, can be used for forecasting, confirm the flare mechanism based on the release of the magnetic energy of the current sheet. For example, the precursor according to which the probability of appearing a flare is significantly increased in the region with alternating spots of opposite polarity compared to regions with the uniform magnetic field, where there are only two spots of opposite polarity or all spots of the same polarity are located in one part of the region. When alternating the polarities of the sources of the magnetic field on the solar surface, singular lines appear in the corona, near which current sheets are formed.

Improving the quality of the forecast of solar flares is necessary from a practical point of view, due to a certain harmful action of flares on human vital activity. Radio emission from flares can interfere with navigation. Induction electric fields at long distances, which arise as a result of magnetic substorms caused by solar flares, can damage transformer stations and other electrical equipment, sometimes even damage power lines (although it must be recognized that such cases are extremely rare). Cosmic rays and X-ray emission caused by solar flares can cause irradiation of cosmonauts, if precautionary measures are not taken. Long-term experience have shown the absence of any significant effect of solar flares on human health, so there is no need to artificially exaggerate this effect in order to draw attention to the problem. In addition to practical value, an understanding of the physics of an interesting explosive process will enrich our understanding of the phenomena occurring in space and laboratory plasma.

According to the hypothesis of S.I. Syrovatsky [2], the appearance of a flare in the corona can be explained by the accumulation of the energy in the magnetic field of the current sheet. A sheet is formed in the vicinity of a singular line of the X-type magnetic field under the action of perturbations propagating from the photosphere. The magnetic forces $\mathbf{j} \times \mathbf{B}/c$ cause plasma motion, which deforms the magnetic field into the configuration corresponding to the current sheet. After quasi-stationary evolution, during which the total plasma mass of the sheet decreases due to the rapid leakage of plasma from the sheet under the action of the magnetic tension [3, 4], the current sheet becomes unstable, and its magnetic energy is explosively released.

At present, a number of alternative solar flare mechanisms have been proposed, however, apart from the mechanism of energy release of the current sheet, the authors are not aware of other mechanisms that could explain the slow accumulation of the energy in a stable configuration, and then its transition to an unstable state in the real active region. From all proposed flare mechanisms, only the current sheet mechanism can explain the slow accumulation of magnetic energy in the stable configuration in the corona, which cannot be destroyed in the process of energy accumulation and, then, the flare release of the accumulated energy when transformation the system into an unstable state.

The most popular alternative mechanism explains the flare by the appearance of a magnetic rope with current [5]. According to these ideas, the rope is accelerated upward with magnetic force $\mathbf{j} \times \mathbf{B}/c$, which leads to the plasma ejection and flare energy release. To simulate this process, most often from the very beginning an unstable or nonequilibrium configuration with the magnetic rope is specified. Attempts to obtain the rope in the corona as a result of the evolution of the magnetic field under the action of perturbations in the photosphere were carried out in [6–8]. In [6], the rope was obtained by twisting the bases of the magnetic arch. After twisting exceeding the threshold (4π), kink instability arose, however, for appearance of this situation above the active region, the twisting speed should exceed the observed rotation speed of the spots by an order of magnitude. In [7, 8], when setting the MHD simulation problem, the initial magnetic field specified by two magnetic charges is extremely simplified compared to the field of the flare active region, and the plasma motion in the photosphere, which leads to the required field deformation in the corona, was set so complex that it is difficult to imagine the implementation in the photosphere in the active region of the Sun. In addition, in order to appear the rope in this situation, it is impossible to do without reconnecting, and hence the current sheet, without which reconnecting is impossible. The very appearance of the current sheet already means the possibility of the flare and, therefore, in this case, the rope is not needed for the flare. Even in this unnatural situation, which is unclear how it can be obtained above the real active region, the flare energy release should occur in the current sheet.

To clarify the flare mechanism, the MHD simulation was performed above the real active region, when all conditions were taken from observations, and no assumptions about the flare mechanism were made

when setting the conditions. The purpose of this simulation is to establish the flare mechanism. The proposed approach was different from that used earlier, when from the very beginning a hypothesis was put forward on the flare mechanism, which was then tested. From all proposed mechanisms, flares of only current sheet are obtained as a result of numerical MHD simulation in the corona above the active region, when all conditions for the formulation of the problem are taken from observations. The simulation proposed in this paper showed the coincidence of the position of the found current sheet with the position of the observed source of thermal X-ray emission.

Recently, a Chinese-American group simulated a flare situation using a supercomputer in a problem close to our conditions setting [9] and confirmed our results. A current sheet appeared at the place of the flare energy release, the magnetic field lines near it are in good agreement with the lines obtained from images of UV emission near the flare region. At the same time, the appearance of ropes or any other indications of alternative flare mechanisms, was not detected, like ours. The fundamental difference between the methods used by us is the development and use of a graphical system for searching for current sheets, which allows us to find and study the flare configuration for not very large flares, when a simple analysis of the magnetic field does not allow us to determine the place of magnetic energy accumulation for the flare due to the presence of the significant field component along a singular line. In [9], the authors studied large X3.1-class flare occurred on October 24, 2014 in the NOAA 12192 active region, which dimensions exceeded the dimensions of all active regions over the past 25 years, so that the current sheet could be found directly from the calculated field configuration.

The available simulation results in the corona above the active region are an independent additional confirmation of the flare mechanism based on the release of the magnetic energy of the current sheet.

2. MAGNETIC FIELD ON THE SOLAR SURFACE BEFORE AND DURING FLARES

Since, according to numerous considerations, the primary release of the magnetic energy of the flare occurs high in the corona, it becomes necessary for simulating numerically MHD to establish the configuration of the magnetic field in the corona, which cannot be obtained from observations. However, some information on the flare mechanism can be obtained from the directly measured magnetic field distribution on the solar surface, since the field in the corona is largely determined by currents under the solar surface. To study the influence of the magnetic field of the active region on solar flares [10–12], we used the measured distributions of the magnetic field component directed along the line of sight (LOS) on the solar surface in the active region. To analyze flares and preflare situations in the regions of AR 10486, AR 10365, and AR 10720, the data of the Michelson Doppler Imager (MDI) instrument of the *Solar and Heliospheric Observatory* (*SOHO*) spacecraft were used (http://soi.stanford.edu/magnetic/index5.html), which mapped every ~1.5 h the field along LOS with the resolution of ~2 heliocentric arc sec (~1000 points along the diameter of the solar disk). To analyze the AR 11158 and AR 11429 regions, we used the data from the Helioseismic and Magnetic Imager (HMI) instrument of the *Solar Dynamics Observatory* (*SDO*) spacecraft (http://jsoc.stanford.edu/ajax/lookdata.html), which mapped every 45 s the field along LOS with the resolution of ~0.5 heliocentric arc sec (~4000 points along the diameter of the solar disk). Since the flare lasts several dozens of minutes (in some cases, the flare duration can be up to 3 h), it was possible to obtain some information on the behavior of the magnetic field in the photosphere during the flare based on the *SOHO*/MDI data only for some successfully occurring flares. *SDO*/HMI representing the magnetic map every 45 s provided ideal information that allowed us to trace the behavior of the magnetic field in the photosphere over the entire duration of the flare. *SDO*/HMI also measured the distribution of all three components of the magnetic field in the photosphere. However, these distributions are derived with the longer time interval, and the component perpendicular to LOS is measured with less accuracy. In view of these circumstances, the distribution of all three field components was not used in the proposed analysis. In addition, the available measurements of the field component along LOS make it possible to have sufficiently good information about the behavior of both the component of the magnetic field normal to the photosphere and the component parallel to the photosphere based on the behavior of the component along LOS. The behavior of the field component parallel to the photosphere can be studied for flares located west of W20 or east of E20 (more than 10 flares were studied for regions having this position), for which the contribution to the measured value is more than 30% of the field component parallel to the photosphere. The study turned out to be especially convenient due to the constancy over time of the distribution of the field component along LOS during the flare, which means the constancy of the components both normal and parallel to the photosphere, since any significant variations in at least one of these components for flares west of W20 or east of E20 would lead to variations in the measured component along LOS (for flares near the center of the disk, the constancy of the component along LOS means the constancy of the component normal to photosphere).

Perhaps in the future, for more detailed studies, it will be possible to use the *SDO*/HMI data on the behavior of the distributions of all three components of the magnetic field in the photosphere. But it is necessary to exercise caution, knowing that the compo-

nent perpendicular to LOS is most likely to be measured less accurately, and it is desirable to have information about the accuracy of its measurement.

The calculation of magnetic fluxes in the photosphere according to measurements of field component distributions along LOS has become possible due to the fact that the magnetic field in the photosphere is determined mainly by currents under the photosphere, rather than currents in the corona. The study, which showed the invariance of the magnetic field in the photosphere during flares, when significant current in the corona ($\sim 10^{11}$ A) and the magnetic field of this current disappear, provides additional evidence that the field in the photosphere is determined by the currents under the photosphere. In this situation, the distribution of all three components of the magnetic field vector in the photosphere coincides with the distribution of the potential magnetic field in the photosphere. The potential field was found from the measured distribution of the field component along LOS in the photosphere. For this purpose, in the corona above the active region, the Laplace equation for the magnetic field potential φ_B with oblique derivative as a boundary condition at the photospheric boundary was numerically solved:

$$\Delta\varphi_B = 0; \quad \left.\frac{\partial\varphi_B}{\partial l_{sight}}\right|_{\text{PhBoun}} = -B_{sight}; \quad \mathbf{B} = -\nabla\varphi_B. \qquad (1)$$

Here, $\partial/\partial l_{sight}$ is the derivative along LOS, B_{sight} is the component of the magnetic field measured in the photosphere. The potential φ_B must satisfy to the condition of equality to zero at infinity, which was approximated by the following two versions for setting the boundary conditions at far removed non-photospheric boundary:

(1) The normal component at the entire non-photospheric boundary of B_{NPhB} is set constant. It is calculated from the condition that the total magnetic flux through the entire boundary of the computational area is equal to zero (the incoming flux is equal to the output). For Laplace equation (1), the condition $\partial\varphi_B/\partial n = B_{\text{NPhB}}$ is set on the non-photospheric boundary.

(2) The potential φ at the non-photospheric boundary was set equal to zero.

The calculations showed that the difference between solutions with both boundary conditions is not significant. Since the potential field was also found with the goal of setting the initial condition for solving the MHD equations in the corona, the Laplace equation was approximated by a finite-difference scheme on the grid for the finite-difference scheme of MHD equations conservative with respect to the magnetic flux.

For all regions, a rectangle with dimensions of 4×10^{10} cm was chosen as the region in the photosphere, which included the active region, in most cases several times exceeding it in dimensions.

For all studied regions, the behavior of the magnetic field before flares (Fig. 1) and during flares (Figs. 1 and 2) is practically the same. A few days before the flare, a slow increase in the fluxes of both the northern (directed toward us) component of the magnetic field and the southern (directed away from us) component of the magnetic field is observed. When the flux reaches the value exceeding $\Phi = 10^{22}$ Mx, large solar flares occur (Fig. 1). During the flare, the magnetic flux remains almost unchanged. The most distinct invariance of the distributions of all field components over time is shown in Fig. 2 for flare X5.4 N18E31 in AR 11429. During the 22-min increase in the intensity of X-ray emission, the northern magnetic flux decreased by ~2%, and the southern one increased by ~0.5%. The *SDO*/HMI data obtained every 45 s were used here. A similar behavior of the studied distributions of the field components for other studied flares indicates the invariance of the magnetic field on the solar surface during flares.

The studied 16 flares in 5 active regions showed the absence of variations in the normal component of the magnetic field in the photosphere. The constancy of the field component along LOS for more than 10 flares located west of W20 or east of E20, for which the contribution of the component parallel to the photosphere to the field component along LOS is more than 30%, means that there are no variations in the distributions of the field component parallel to the photosphere. The absence of variations in the distribution of the magnetic field in the photosphere during flares is independent evidence of the appearance of the flare in the corona, where the disappearance of the magnetic field when releasing the magnetic energy does not affect the field in the photosphere.

3. STUDY OF PLASMA HEATING IN THE CORONA BEFORE AND DURING FLARES BY AN ANALYSIS OF OBSERVATIONS IN UV LINES OF HIGHLY IONIZED IRON

Ultraviolet emission in the lines of highly ionized iron ions arises in high-temperature plasma (5–20 MK), which appears in the solar corona during preflare plasma heating and the flare due to magnetic field dissipation. Therefore, the analysis of emission in the lines of highly ionized iron helps to study the process that occurs before and during the flare. In addition, this analysis will be required in the future to compare the places of preflare energy accumulation and the flare with the position of the flare found in the magnetic field configuration obtained by the MHD simulation in the corona above the active region.

The most convenient for flare analysis are the shortwave UV channels of 94, 131, and 193 Å. The 94 Å channel belongs to the Fe XVIII ion and corresponds to the temperature of 6.3 MK. The 131 Å channel is emitted by plasma with the temperature of 10 and

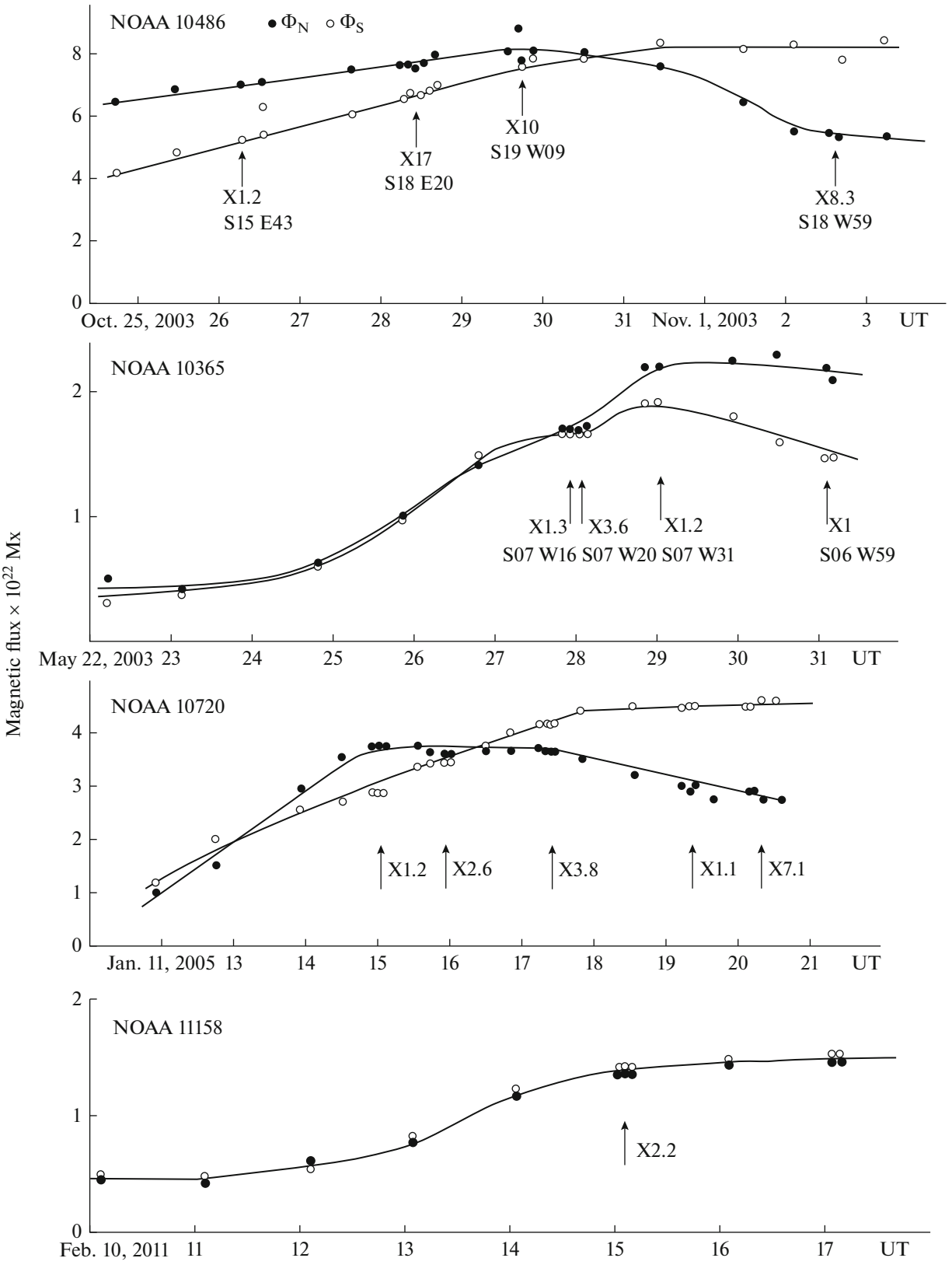

Fig. 1. Dynamics of typical active regions giving powerful solar flares. Arrows indicate the time of flares.

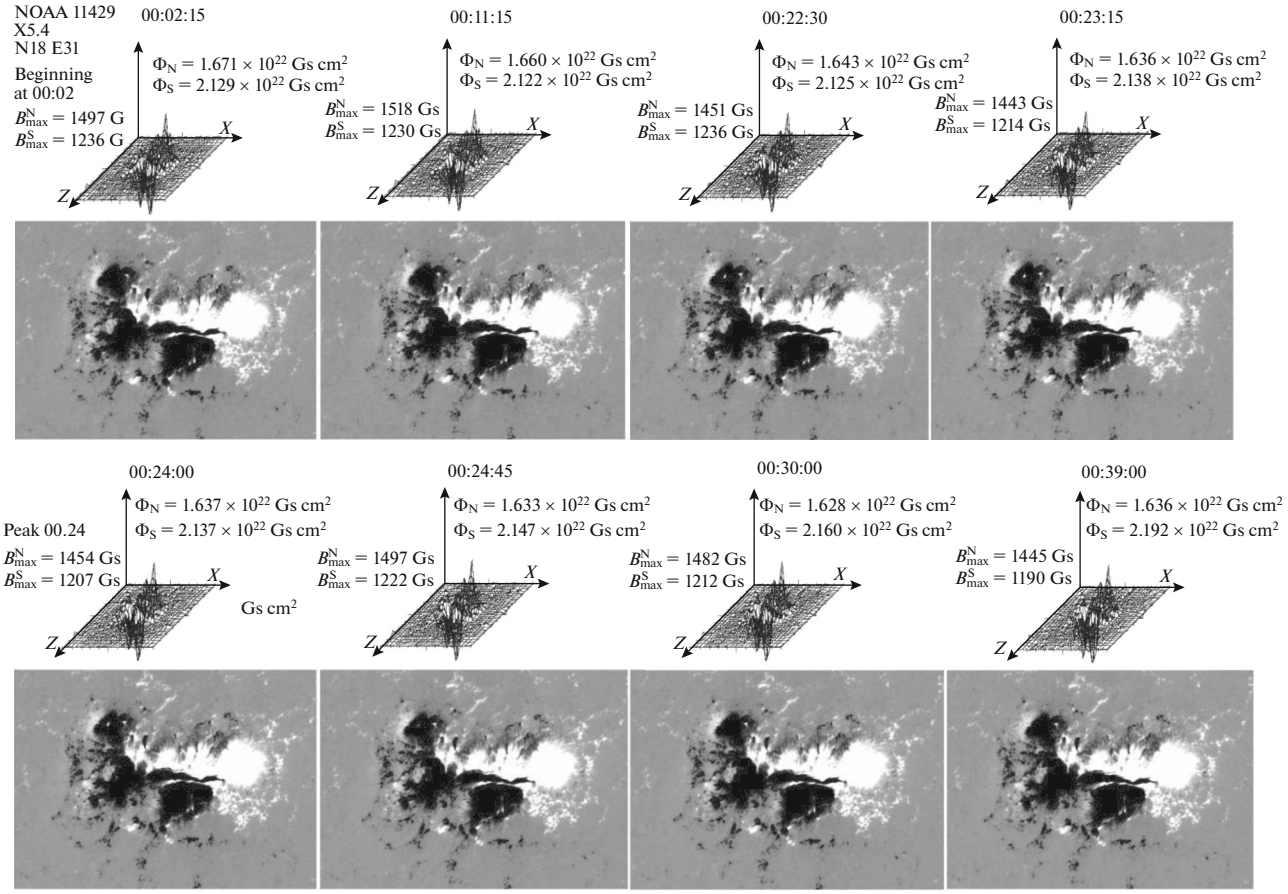

Fig. 2. Distributions of the normal component of the magnetic field and the magnetograms of the X5.4 flare that occurred on March 7, 2012 in active region AR 11429. The scale along the vertical axis for the distribution of the normal component of the magnetic field is $B = 2500$ Gs.

16 MK, and the 193 Å channel contains the emission from plasma with the temperature of 1.2 and 20 MK. If the solar flare occurred in the chromosphere at the low temperature characteristic to the chromosphere, photographs in the spectral lines of 94, 131, and 193 Å would not show a sharp increase in the brightness of the image in the corona during the flare. An increase in the brightness of the structure emission observed in the spectral lines of 94, 131, and 193 Å in the corona during flares should indicate the development of the flare in a high-temperature rarefied corona plasma.

The development of the flare is well demonstrated in the spectral lines of highly ionized atoms [13, 14] detected by the Atmospheric Imaging Assembly (AIA) instrument on the *SDO* spacecraft (https://sdo.gsfc.nasa.gov/data). A typical development of a solar flare is shown in Fig. 3. The frames obtained before the flare are shown at the left of the vertical dashed line. The X3.1 flare arose above the active region in the central part of the solar disk on October 24, 2014 at $t_0 = 21{:}07$. This figure shows the development of the flare at the right of the vertical line. The first row shows one of the most fundamental properties of the flare: the practical constancy over the course of an hour and a half of the distribution of the sources of the photospheric magnetic field immediately before and during the flare. The second row shows a very weak increase in the emission of the hot plasma at 193 Å of Fe XXIV before the flare, but its sharp increase during the flare. The third line (131 Å of Fe XXIII) also demonstrates the beginning of heating of coronal plasma cloud during the formation of the current sheet above the active region and the rapid heating of plasma during the flare. The fourth row indicates the preliminary heating the coronal plasma cloud when forming the current sheet and the development of the emission of the 94 Å of Fe XVIII during the flare. The fifth row shows the chromospheric structures that are the result of an explosive process in the corona: flare ribbons, which have long been considered the main manifestations of the flare.

In the photographs taken before the flare on September 10, 2014 (Fig. 4) in the 94 Å channel, one can see a luminous structure, which shape clearly does not correspond to the shape of individual magnetic lines above the active region, which are clearly manifested

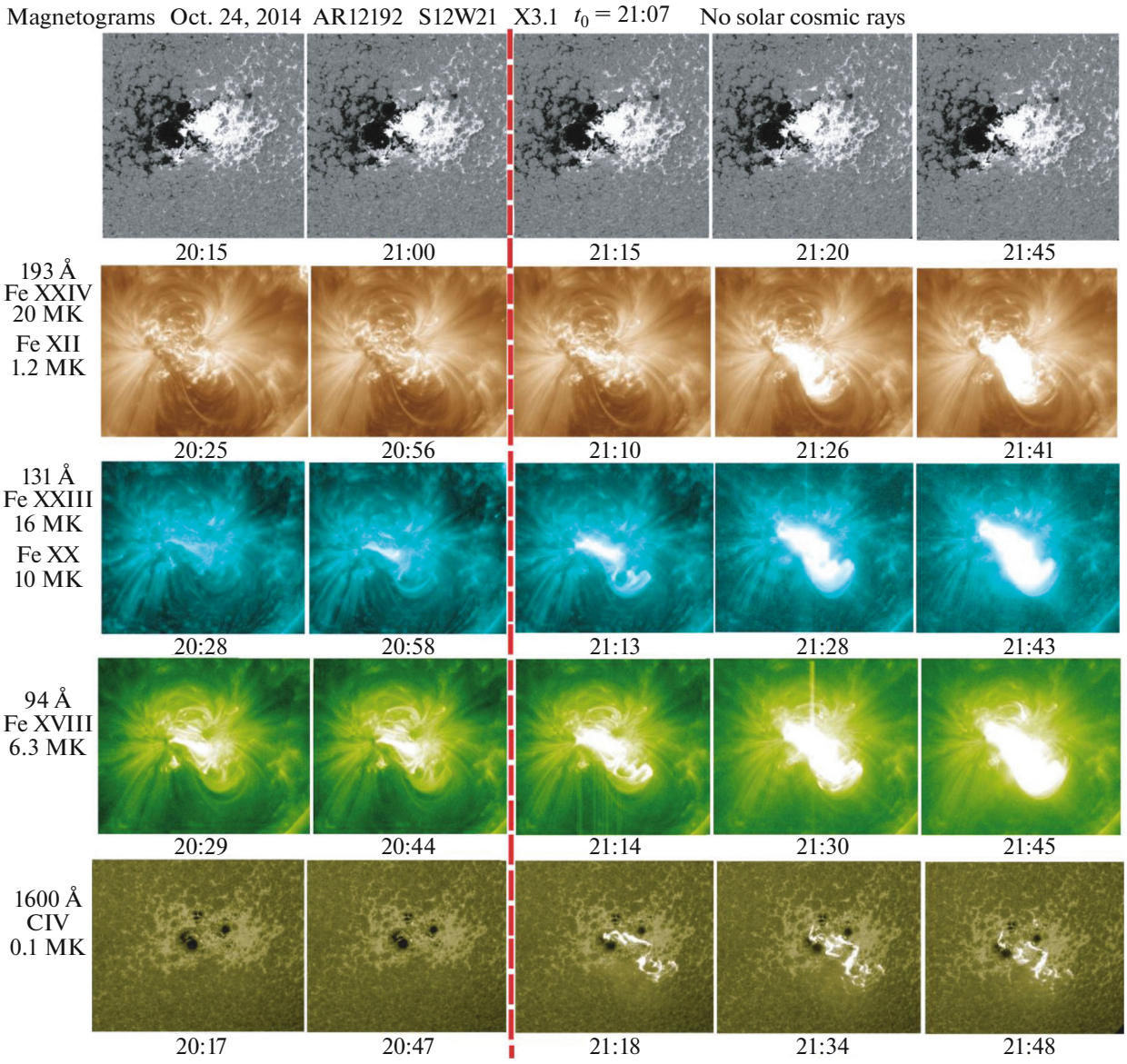

Fig. 3. Emission of ions of different ionization rates in the preflare state and during the flare that occurred in the middle of the solar disk.

in these photographs. A local preflare emission in the 94 Å channel shows the appearance of a hot preflare structure, which temperature significantly exceeds not only the temperature of the chromosphere, but also the corona, therefore, the preflare process develops in the corona above the active region, and not in the chromosphere. The typical dimension of the local preflare region is about 10^{10} cm. This preflare structure appears in front of half of the large flares in 10–30 h, i.e., when the numerical MHD simulation shows the formation of the current sheet above the active region and the accumulation of magnetic energy in it [4, 15, 16], which can release during flare. Before the flare, the brightness of the luminescence of the channel 94 Å gradually increases, and then during the flare the luminescence of this line increases rapidly. The 131 Å channel and especially the 193 Å channel containing plasma emission corresponding to temperatures of 16 and 20 MK behave somewhat differently. The emission in these lines before the flare is very weakly expressed, and its structure varies rapidly, in contrast to the clearly defined structure of the 94 Å channel emission in the preflare state. Varying images in the 131 and 193 Å channels cannot be identified. For weak emissions in high-temperature lines of 131 and 193 Å, it is impossible to speak of any specific preflare structure. This means that the plasma temperature in preflare states does not reach the temperature of ~20 MK. However, as follows from Fig. 4, emissions of high-temperature lines, especially the 193 Å channel, increase sharply

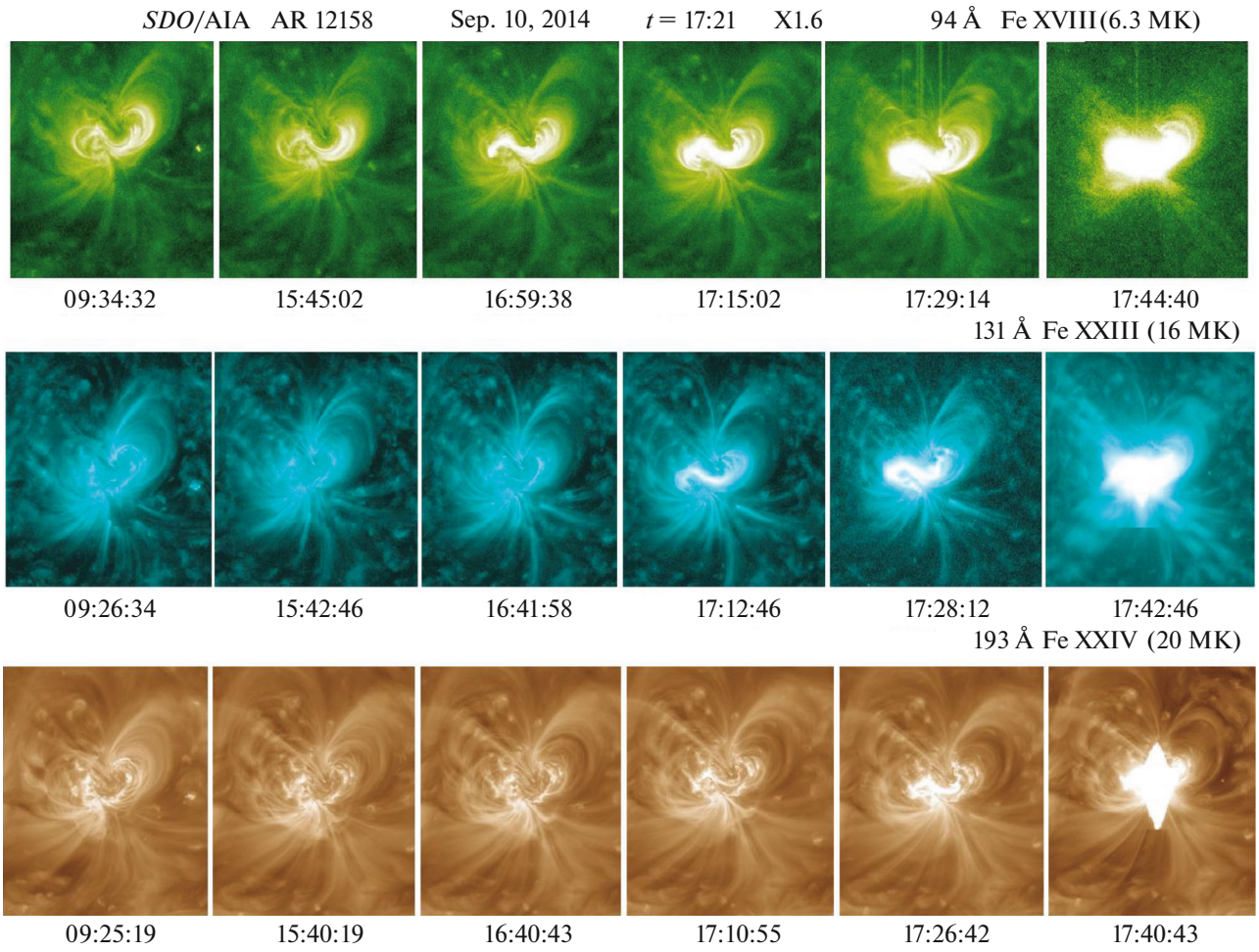

Fig. 4. Emission of active region AR 12158 in channels 94, 131, and 193 Å before and during the X1.6 flare.

during the flare. The appearance on the solar disk of the clearly manifested preflare emission in the 94 Å channel can serve as an indication for forecasting large flares.

4. STUDYING THE FLARE SITUATION BY NUMEROUS MHD SIMULATION IN THE CORONA OVER THE REAL ACTIVE REGION

At present, the configuration of the magnetic field in the corona above the real active region cannot be determined from observations. To determine the configuration of the field, velocity distributions, plasma density, and temperature, numerical MHD simulation was performed, in which all conditions were taken from observations. When setting the conditions, no assumptions about the solar flare mechanism were made. The aim of simulation is to define the solar flare mechanism. There are serious considerations that the flare mechanism is associated with the release of energy accumulated in the field of the current sheet, but in this case, the numerical MHD simulation above the real active region should establish the mechanism of the solar flare regardless of what is the mechanism (current sheet, magnetic rope or some other, perhaps no one has yet proposed mechanism). To set the boundary simulation conditions, we used the magnetic field distributions observed in the photosphere. The calculation began several days before the flare, when strong disturbances were absent, and, therefore, the potential magnetic field in the corona calculated from the observed field distribution in the photosphere, can be used to set the initial conditions. All other conditions at both the photospheric and non-photospheric boundaries were approximated by the free exit conditions.

The simulation was carried out for the active region of AR 10365, which gave a series of flares on May 27, 2003. To take into account all features of the field, the simulation was carried out in the computational domain with dimensions of 4×10^{10} cm several times larger than the dimension of the active region. To find the potential field, the Laplace equation (1) was numerically solved with the oblique derivative as the boundary condition. For this purpose, we used maps

of the magnetic field component along LOS in the photosphere obtained by the *SOHO*/MDI instrument (http://soi.stanford.edu/magnetic/index5.html).

The MHD equations were solved numerically in the computational area ($0 \le x \le 1$, $0 \le y \le 0.3$, $0 \le z \le 1$, in dimensionless units). The unit of length was chosen equal to $L_0 = 4 \times 10^{10}$ cm. The Y axis is directed away from the Sun normally to the photosphere. The XZ plane ($y = 0$) is the photosphere plane with the X axis directed from east to west and the Z axis directed from north to south. The characteristic value of the field in the active region $B_0 = 300$ Gs was chosen as the unit of the magnetic field. The dimensionless units of plasma concentration and its temperature are taken to be their typical values in the corona above the active region, which are assumed to be constant in space at the initial moment: $\rho_0/m_i = 10^8$ cm^{-3}, $T_0 = 10^6$ K (m_i is the ion mass). The dimensionless units of velocity, time, and current density have the form: $V_0 = V_A = B_0/\sqrt{4\pi\rho_0}$, $t_0 = L_0/V_0$, $j_0 = cB_0/4\pi L_0$. The three-dimensional dimensionless system of MHD equations has the form:

$$\frac{\partial \mathbf{B}}{\partial t} = \mathrm{rot}(\mathbf{V}\times\mathbf{B}) - \frac{1}{\mathrm{Re}_m}\mathrm{rot}\left(\frac{\sigma_0}{\sigma}\mathrm{rot}\mathbf{B}\right), \tag{2}$$

$$\frac{\partial \rho}{\partial t} = -\mathrm{div}(\mathbf{V}\rho), \tag{3}$$

$$\frac{\partial \mathbf{V}}{\partial t} = -(\mathbf{V},\nabla)\mathbf{V} - \frac{\beta_0}{2\rho}\nabla(\rho T) - \frac{1}{\rho}(\mathbf{B}\times\mathrm{rot}\mathbf{B}) + \frac{1}{\mathrm{Re}\rho}\Delta\mathbf{V} + G_g\mathbf{G}, \tag{4}$$

$$\begin{aligned}\frac{\partial T}{\partial t} &= -(\mathbf{V},\nabla)T - (\gamma-1)T\mathrm{div}\mathbf{V} + (\gamma-1)\\ &\times\frac{2\sigma_0}{\mathrm{Re}_m\sigma\beta_0\rho}(\mathrm{rot}\mathbf{B})^2 - (\gamma-1)G_q\rho L'(T)\\ &+\frac{\gamma-1}{\rho}\mathrm{div}\left(\mathbf{e}_\parallel\kappa_{dl}(\mathbf{e}_\parallel,\nabla T) + \mathbf{e}_{\perp 1}\kappa_{\perp dl}\right.\\ &\left.\times(\mathbf{e}_{\perp 1},\nabla T) + \mathbf{e}_{\perp 2}\kappa_{\perp dl}(\mathbf{e}_{\perp 2},\nabla T)\right).\end{aligned} \tag{5}$$

The limitations associated with the finite step of the difference scheme do not allow us to use real values of dimensionless parameters in the diffusion terms of Eqs. (2)–(5), therefore, the principle of limited simulation was used to select the parameter values [17]. According to this principle, dimensionless parameters much larger and much smaller than one are specified in the calculations much larger and much smaller than one without the exact preservation of their values. The following parameter values were used in the calculations: $\gamma = 5/3$, $\mathrm{Re_m} = 1000$, $\mathrm{Re} = 300$, $\beta_0 = 0.6 \times 10^{-5}$, $\Pi = 100$, $\Pi_B = 10^4$, $G_q = 0.3 \times 10^{-5}$. The gravitational force can be neglected in comparison with the magnetic force and plasma pressure force: $G_g = 0$.

For the numerical solution of the system of MHD equations, an absolutely implicit scheme, which is conservative with respect to magnetic fluxes, has been developed. This scheme allows one to obtain stable solutions in the active region of the corona [18]. The scheme is implemented in the PERESVET code. The high stability of the scheme is ensured by the fact that both the dissipative terms and the transfer terms were taken at the next time step ($j + 1$), and in this case, the first-order approximation of the transfer terms was carried out by asymmetric upwind finite differences. The scheme was solved by the iteration method. Good convergence of iterations was ensured by the fact that the values at the central stencil point included in the finite-difference analogues on the right side of equations were taken at the next iteration [19].

When solving MHD equations at the photospheric boundary, it is necessary to specify two field components parallel to the boundary. The component perpendicular to the boundary is determined from the condition $\mathrm{div}\mathbf{B} = 0$. Therefore, if there is observational data only regarding the field component along to LOS, then it is necessary at different times to find two field components parallel to the boundary from the potential field, solving Eq. (1). Setting ρ, **V,** and T on the entire boundary and parallel to the boundary of the **B** components on the non-photospheric boundary was approximated by the free exit conditions. The field component perpendicular to the boundary was determined from the condition $\mathrm{div}\mathbf{B} = 0$. The distributions of two components of the magnetic field parallel to the photosphere were found from the potential magnetic field calculated from the field distributions along LOS from the *SOHO*/MDI magnetograms at the times of May 24, 2003 on 20:47:59; May 25, 2003 on 20:47:59; May 26, 2003 on 20:47:59; May 27, 2003 on 20:47:59 UT. The boundary conditions at each time instant were found by interpolating between these time instants. This interpolation can be used since magnetic fluxes and magnetic field distributions in the photosphere vary rather slowly [10–12].

Despite the application of specially developed methods, the MHD simulation in the corona above the active region is carried out so slow that it was possible to carry out the calculation for the active region 10365 on a regular computer only in a very shortened time scale (the magnetic field under the conditions specified at the boundary varied 10^4 times faster than on the photosphere of the Sun). In this calculation, as a result of an unnaturally rapid variation in the field at the photospheric boundary, a numerical instability arises, which distorts the solution. However, the used methods made it possible to prevent the instability from spreading inside the computational area from the photospheric boundary and to limit the growth of values in the boundary region so that calculation is possible.

In the general case, the magnetic field on the singular line should not be zero and the singular line should not be straight. Therefore, the configuration of the magnetic field in the vicinity of the current sheet

formed in the vicinity of the singular line can be so complicated that using the shape of the magnetic lines it is impossible to determine the position of the current sheet found by numerically solving MHD equations. To determine the position of the current sheet (flare position) in the configuration of the field found using the MHD simulation, which is actually the location of the flare, the graphic search system is developed that also visualizes the solution of MHD equations. The method of flare position search is based on the fact that, regardless of the coordinate system, the local maximum of the absolute value of the current density is located in the middle of the current sheet. The maxima of the current density are searched, and then an analysis of the magnetic field configuration is carried out near them. A detailed description of the flare position search system can be found in [20].

Using the developed search system, it was possible to determine the position of the M1.4 flare on May 27, 2003 at 02:40 based on the results of the MHD simulation. The flare was located at the altitude of 16000 km. The position of the maximum current density for the current sheet at the time of the flare of (0.46, 0.04, 0.445) in dimensionless coordinates is shown in Figs. 5a and 5b in the plane parallel to the photosphere and the plane perpendicular to the photosphere crossing the photosphere along the solar equator. Figure 5d shows a fairly good agreement in the picture plane (perpendicular to LOS) of the found flare position (on the disk $(x, y) = (96'', 56'')$ in arc sec of the heliocentric coordinate system) with the position of the thermal X-ray source (99″, 64″). A slight difference can appear due to the uncertainty of time, when simulating on the reduced time scale. In the plane passing through the point of maximum current density and located perpendicular to the magnetic field vector at this point (perpendicular to the tangent to this vector of singular field line), the magnetic configuration corresponding to the current sheet is most pronounced. We will call this plane the configuration plane of the current sheet. Figure 5c in the plane of the photosphere gives an idea on the location of the configuration plane of the current sheet for the M1.4 flare: the line of crossing of the configuration plane with the photosphere is shown and the arrow shows the direction of inclination of 18° of the configuration plane to the photosphere.

Field configuration in Figs. 6a–6c are represented by flat lines, since it is almost impossible to get an idea of the field configuration from the complex arrangement of the magnetic field lines in the three-dimensional space near the current sheet. The process of formation of the current sheet, as well as the process of rapid field dissipation during instability of the sheet, is largely determined by the magnetic forces $\mathbf{j} \times \mathbf{B}/c$ that causes the plasma motion, which deforms the magnetic field. Since the main current in the sheet is directed along the singular line of the magnetic field the component of the magnetic field perpendicular to the configuration plane and parallel to the singular line will be parallel to the current and therefore will not contribute to the magnetic force $\mathbf{j} \times \mathbf{B}/c$. The magnetic force will be determined by the components of the magnetic field in the plane of the configuration of the current sheet, i.e., vectors that are projections of the magnetic field vector onto the configuration plane. The main processes in the current sheet are determined by the projections of the magnetic vectors onto the plane of the configuration of the current sheet, i.e., lines tangent to the projections of the magnetic vectors onto the configuration plane. The magnetic force vectors $\mathbf{j} \times \mathbf{B}/c$ will be located in the configuration plane perpendicular to these lines. The lines tangent to the projections of the magnetic vectors onto the configuration plane and the planes parallel to it are shown in Figs. 6a–6c. Figures clearly show that these lines form the deformed X-type configuration near the current sheet. Figures 6d and 6e give an idea of the shape of regions with high current during flare.

The coincidence of the found position of the current sheet for the flare on May 27, 2003 at 02:40 in the magnetic configuration obtained by the MHD simulation above the real active region with the position of the flare thermal X-ray source is an independent proof of the mechanism of the solar flare based on the release of energy accumulated in the magnetic field of the current sheet. Studying the magnetic field configuration near the current sheet in the corona above the active region 10365 for the flare on May 27, 2003 at 02:40 showed that the physical meaning of the processes of accumulation and rapid release of the flare energy reflects not magnetic lines of force, but lines in the plane of the current sheet configuration tangent to the projections of the magnetic field vectors onto this plane. The location of these lines, which have opposite directions on both sides of the sheet, corresponds to the existence of forces that create the current sheet, and then are able to destroy it, when the system transforms into an unstable state. The proposed methods of the MHD simulation and search for the positions of current sheets and visualization will be needed to further refine the position of flares and field configuration using calculations in the real-time scale.

5. ELECTRODYNAMIC MODEL OF SOLAR FLARE

The electrodynamic model of a solar flare (Fig. 7) [15, 21] was proposed based on the results of the numerical MHD simulation in the corona above the active region and comparison of simulation results with observations. The model explains the main observational manifestations of the solar flare: the appearance in the corona of a source of thermal X-ray emission and a source of UV emission in the lines of highly ionized iron, which is formed in hot plasma; the appearance of sources of hard beam radiation on the solar surface; the appearance of solar cosmic rays:

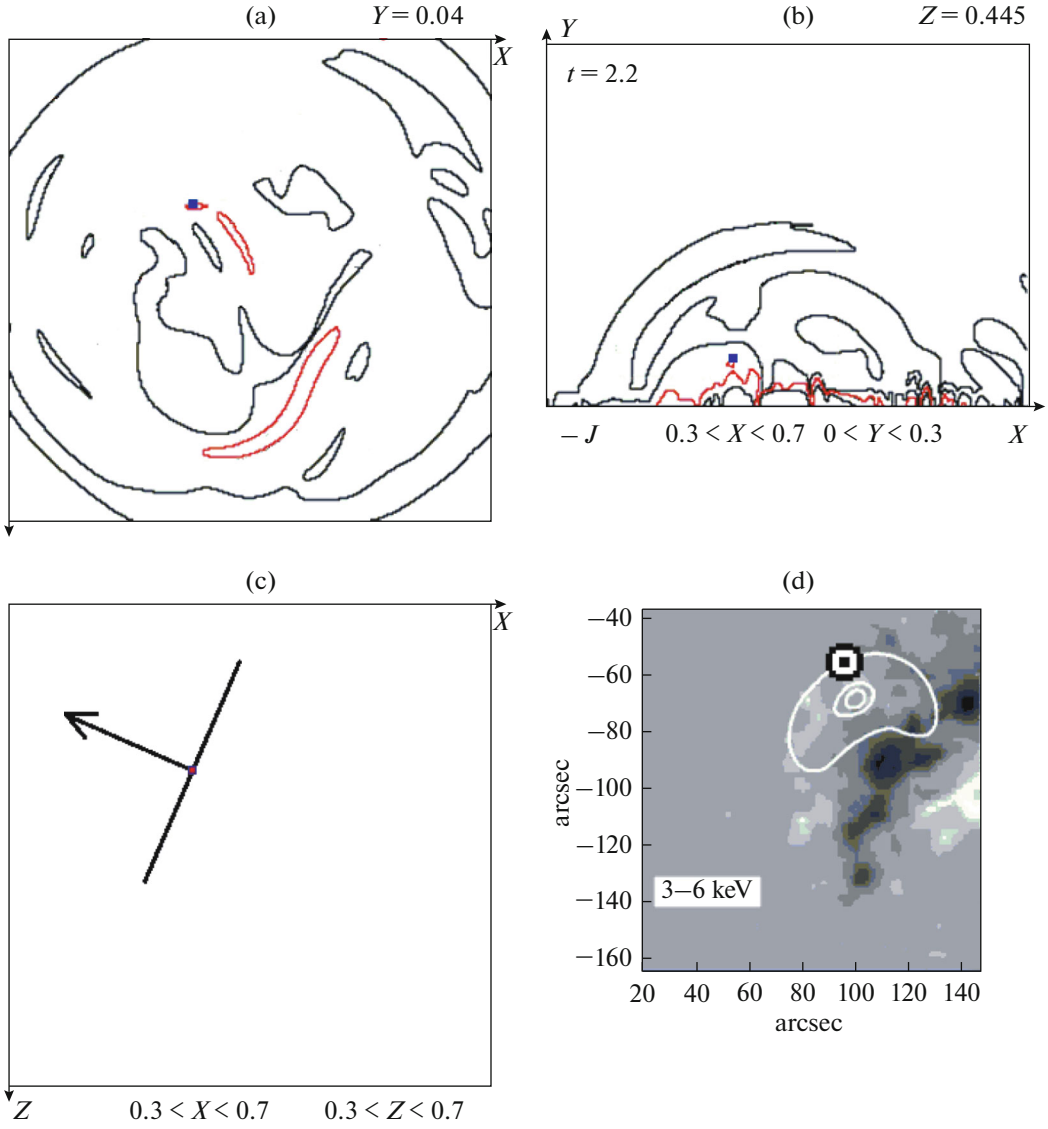

Fig. 5. (a and b) The position of the flare found using MHD simulation (bold point), lines of equal current density are shown. (c) The location of the configuration plane of the current sheet perpendicular to the magnetic field vector **B** = (0.179, 0.066, 0.093) (in dimensionless units) at the point of maximum current density. (d) The found flare position in the picture plane is plotted on the distribution of 3–6 keV thermal X-ray emission obtained on the *RHESSI* spacecraft (http://rhessidatacenter.ssl.berkeley.edu) on May 27, 2003 at 02:53, which is superimposed on the *SOHO*/MDI magnetogram obtained on May 27, 2003 at 03:12.

protons accelerated to energies of ~20 GeV and electrons accelerated to several hundred keV; plasma ejection during the flare; floating afterflare loops; the appearance of several (most often two) H_α ribbons in the photosphere, which diverge during the flare, and similarly behaving ribbons in the visible and UV lines of the photosphere, chromosphere, and transition layer. The occurrence of this set of flare manifestations is a consequence of the explosive release of the magnetic energy of the current sheet during the transition of the current sheet to an unstable state. The dissipation of the magnetic energy stored in the field of the current sheet leads to heating of the plasma in the sheet to 30–50 MK and the appearance of a source of thermal X-ray emission, first recorded on the *Yohkoh* and *RHESSI* spacecraft [1, 22, 23] and a emission source in highly ionized iron channels 94 Å Fe XVIII, 131 Å Fe XXIII, and 193 Å Fe XXIV recorded on the *SDO* spacecraft (https://sdo.gsfc.nasa.gov/data).

The plasma, along with the magnetic field lines, flows into the current sheet from both sides and, after magnetic reconnection in the vicinity of the X-line of the field, is accelerated by the force $\mathbf{j} \times \mathbf{B}/c$ along the sheet. Upward accelerated plasma creates a coronal ejection. The flux of plasma heated during reconnection of field lines downward together with the contracting field lines creates hot postflare loops.

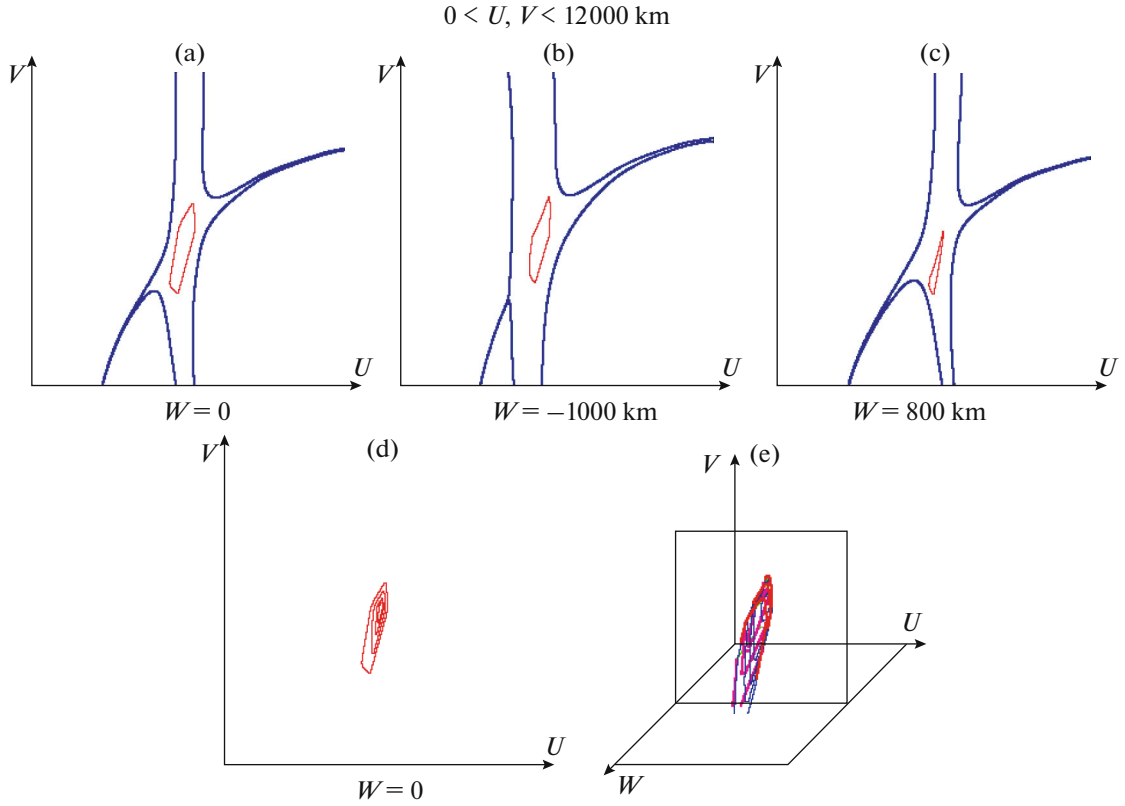

Fig. 6. (a, b, c) The configurations of the magnetic field in the plane of the configuration of the current sheet and two planes parallel to it, lines of equal density are thin. (d) Lines of equal current density in the configuration plane and (e) the surface of equal current density in space with coordinates in the configuration plane and along a singular line.

The Hall electric field directed along the sheet $\mathbf{E} = \mathbf{j} \times \mathbf{B}/nec$ causes a system of field-aligned (parallel to magnetic lines) currents. Field-aligned currents and their directions are shown by bold blue lines. The field-aligned currents directed to the solar surface are closed in the chromosphere by Pedersen currents flowing across the magnetic field. Pedersen conductivity is provided by collisions of charged particles with neutral atoms and the resistance of the low-temperature plasma of the chromosphere. Electrons accelerated in these currents are precipitated on the surface of the Sun and cause the glow of flare ribbons in hard beam X-ray emission. Plasma heating by beams of accelerated electrons leads to the appearance of ribbons in the visible and UV lines of low-temperature plasma of the photosphere, chromosphere, and transition sheet. The locations of the lines in Fig. 7 show that over time, the distance between the intersection points located on the both sides of the current sheet with the photosphere of the magnetic lines, which are reconnected in the current sheet, increases that explains the observed divergence of the flare ribbons. Flare subterahertz emission with the frequency of 400 GHz can be caused at the Langmuir frequency in plasma with the concentration of 10^{15} cm^{-3} by electron beams accelerated in field-aligned currents. Plasma with this concentration exists in the lower dense layers of the solar atmosphere, where the plasma concentration varies from 10^{12} cm^{-3} (chromosphere) to 10^{17} cm^{-3} (photosphere).

Figure 7 also shows upward field-aligned currents caused by the Hall electric field. These currents are propagated along magnetic lines along with the Alfven wave caused by the flux of electrons that carry the main current in the current sheet, into which the magnetic field is frozen. The upward field-aligned currents are closed by displacement currents in the place, to which the Alfven wave has reached at the time instant. Electrons accelerated in upward field-aligned currents in rarefied plasma cause weak hard beam X-ray emission on a thin target, which was recorded in [24] only for a flare above the region located behind the limb. In this case, the powerful hard emission of a thick target on the solar surface is screened by the Sun and therefore does not interfere to observe hard emission in the corona caused by accelerated electrons in upward field-aligned currents. The interaction of these accelerated electrons with interplanetary plasma causes emission at the plasma frequency, III-type radio emission. The acceleration of protons to ultrahigh energies along the X-line of the magnetic field in the direction perpendicular to the plane of the figure in the electric field $\mathbf{E} = -\mathbf{V} \times \mathbf{B}/\mathbf{c}$ is described in detail in Chapter 7.

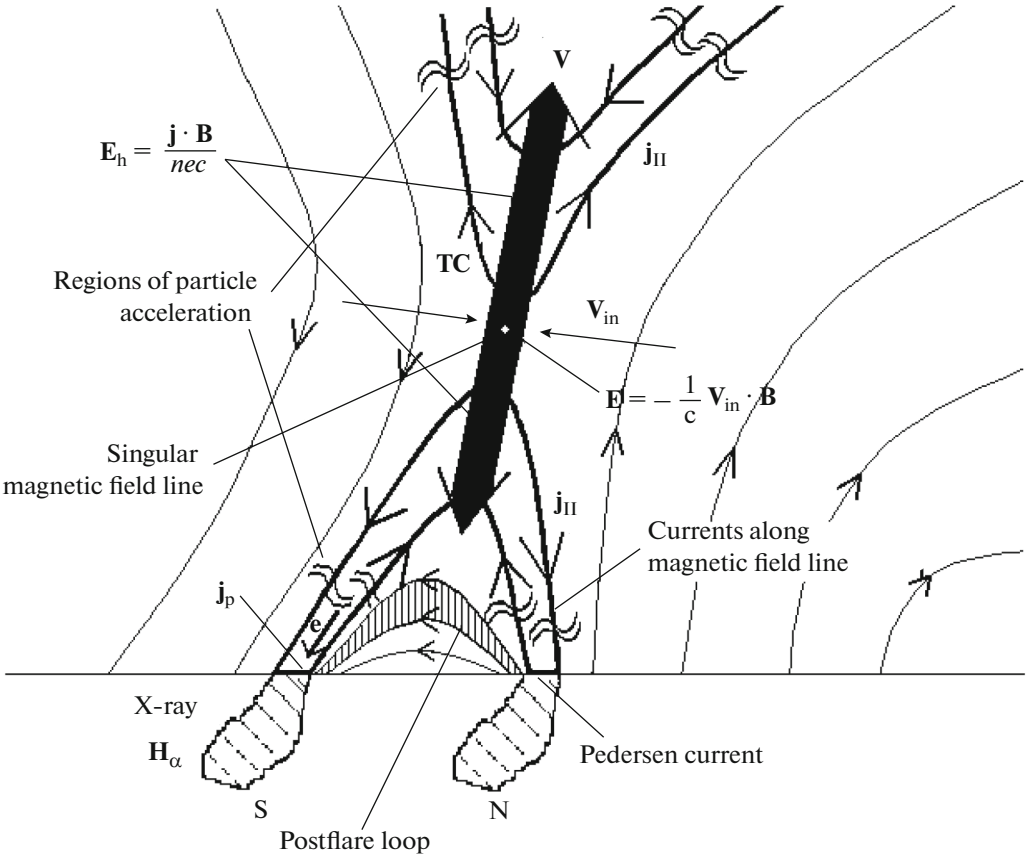

Fig. 7. Electrodynamic model of a solar flare. Thin lines indicate magnetic field lines. Thick lines are currents along magnetic field lines. The bold strip is the current sheet. The vectors show the directions of the plasma flowing into the sheet with velocity V_{in} (this velocity is also called the reconnection velocity). Hall electric field E_h is directed along the sheet up and down. Magnetic tension ejects plasma from the sheet. Flux upward creates a coronal ejection. Flux downward creates a postflare loop.

6. ON THE OPPORTUNITY AND NECESSITY FOR SIMULATING FLARE SITUATION IN THE REAL TIME

For the MHD simulation, a specially developed finite-difference scheme was used, which is stable for sufficiently large steps in order to accelerate the calculations as much as possible. Despite the use of these methods, the simulation in the corona above the real active region is implemented rather slowly. The simulation above AR 10 365 could be performed only on a greatly reduced (10^4 times) time scale, the calculation took ~3 months. An unnaturally rapid variation in the magnetic field led to numerical instability near the photospheric boundary, however, the use of the developed methods did not allow the instability to propagate inside the computational area and limited the development of instability near the photospheric boundary, so that the simulation became possible. This simulation made it possible to establish the appearance of the current sheet that is in good agreement with the observed source of flare thermal X-ray emission. Methods have been developed and tested for the numerical solution of MHD equations, the search for the position of the current sheet and the graphical representation of the solution of MHD equations in the corona. These methods will be needed in the MHD simulation in the real scale of time, which is necessary to clarify the information received so far about the processes leading to a flare in the corona and to obtain information about processes that could not be obtained by numerical simulation in the corona in the reduced scale of time.

MHD simulation in the real scale of time will make it possible to more accurately determine the time of formation and the position of the current sheet for comparison with observations. It will become possible to accurately determine the shape of the region of high current in the picture plane for comparison with the region of hot plasma observed in the lines of highly ionized iron 94 Å Fe XVIII, 131 Å Fe XXIII, and 193 Å Fe XXIV, as well as the energy for the flare accumulated in the magnetic field of the current sheet. The configuration of the magnetic field must be precisely found both in the vicinity of the current sheet and in the region of the corona of significant dimensions containing the current sheet. Here, it will be necessary to pay special

attention to regions near the photospheric boundary, where, in the real-time scale calculation, the field will not be distorted by the instability. This will make it possible to accurately determine the intersection with the photosphere of magnetic lines crossing the current sheet for comparison with observations of hard X-ray emission. In such places, according to the electrodynamic model of the flare, sources of hard X-ray emission should appear. The calculation performed on the reduced time scale, possibly due to instability near the photospheric boundary, did not reveal any clear coincidence of the observed sources of hard X-ray emission with the intersection points of the magnetic lines crossing the current sheet with the photosphere. The calculation results show only the possibility in principle of such coincidence. The electric and magnetic fields precisely determined as a result of real-time scale calculation will make it possible to more accurately study the accelerations of solar cosmic rays by calculating the particle trajectories in the found fields (see Chapter 7). According to observations, solar cosmic rays appear only for ~30% of powerful X-type flares. Calculation of particle motion in the obtained fields obtained by real-scale simulation in the large-sized region will probably determine whether particles accelerated in the current sheet can escape beyond strong magnetic fields above the active region, i.e., whether particles from this flare will appear. The latter is important from a practical point of view to caution cosmonauts in order to take measures against exposure to solar cosmic rays.

The possibility of obtaining all necessary information regarding the flare state in the corona is indicated by the absence of instability at the photospheric boundary, which was shown by real-time MHD simulation carried out during the first 7 min of active region evolution. This also means the absence of local current density maxima resulting from the instability that mask the current sheet and the need for additional study of the field configuration near such maxima in order to understand whether they are the current sheet.

The modeling results of the corona during the first 7 min (Fig. 8) show the beginning of formation of the current sheet. The simulation showed that the calculation of evolution above the active region within 3 days should take ~3 years on an ordinary modern computer.

For MHD simulation of the corona in real time, A.V. Borisenko has adjusted hardware and software for a supercomputer based on the CUDA NVIDIA Tesla M2050 video card [25]. Test calculations of the solution of simple Poisson equation, using a difference scheme similar to the implicit scheme used to solve MHD equations, showed computing acceleration by a factor of 20–150, depending on the details of the choice of the difference scheme and the conditions for choosing a calculation mode carried out in parallel by many video card processors. This computing acceleration will make it possible to carry out MHD simulation in the real scale of time. At present, the numerical solution of MHD equations is being parallelized.

7. ACCELERATION AND DISTRIBUTION OF SOLAR COSMIC RAYS

The Sun is a unique astronomical object that generates proton pulses with an energy of at least 20 GeV, whose origin is accessible to direct study. The acceleration of charged particles to relativistic energies can occur along a singular line of the magnetic field in Lorentz electric field $\mathbf{E} = -\mathbf{V} \times \mathbf{B}/c$, which occurs, when plasma flows into the sheet [26, 27]. The efficiency of particle acceleration by the Lorentz electric field directed along a singular line of the magnetic field follows from laboratory experiments with a powerful pulsed discharge (Fig. 9). These experiments were carried out in connection with the problem of controlled thermonuclear fusion [28]. The measurements showed that during the maximum compression rate of plasma discharge, particles acquire energy greater than 300 keV with a potential difference of about 15 keV applied to the electrodes [29].

To elucidate the nature of the spectrum of particles accelerated in the current sheet, a calculation was performed by the method of test particles [30, 31], which used the field configuration obtained in a three-dimensional numerical MHD experiment for the Bastille flare (July 14, 2000). The calculation showed an exponential index of the spectrum, which coincides with the measured one at the magnetic reconnection velocity of 10^7 cm/s (Fig. 10). Thus, the main parameter of the flare, the magnetic reconnection rate, was estimated.

MHD simulation, as well as the approximate estimates made earlier shows the value of the magnetic field near current sheet $B = 100$ Gs, so that the value of the electric field in the sheet $\mathbf{E} = \mathbf{V} \times \mathbf{B}/c$ is ~20 V/cm, and for sheet length $L = 10^9$, the particle will gain maximum energy of 2×10^{10} eV, following the path along which the potential difference is $E \times L$. This energy corresponds to the maximum observed energy of solar cosmic rays.

Not all solar flares cause the appearance of solar cosmic rays. Only about 30% of X-class flares cause cosmic-ray fluxes. This is explained by the fact that, in many cases, the configuration of the field above the active region holds particles accelerated in the current sheet, preventing them from entering interplanetary space. At present, the Fermi mechanism of acceleration of both galactic and solar cosmic rays on shock waves has become widespread. According to this mechanism, a particle crosses the front of a shock wave several times, reflected from plasma inhomogeneities, and, in this case, gains energy due to the difference in the average velocity of the inhomogeneities on both sides of the shock wave front. For solar cosmic

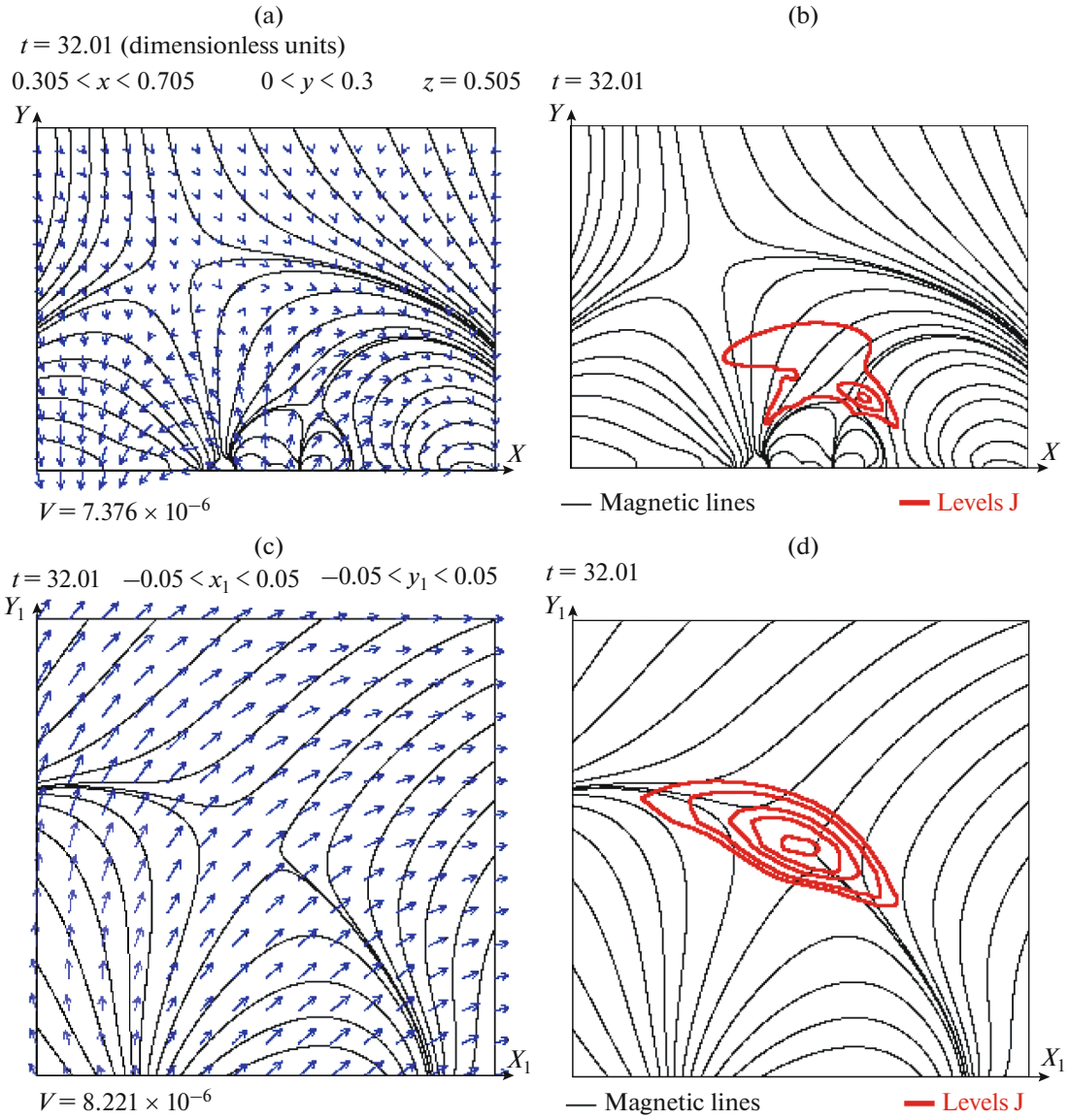

Fig. 8. (a, b) The results of MHD simulation of evolution above active region AR 10365 in real time at time $t = 7.5$ min in the central plane $z = 0.505$, and (c, d) in planes containing points of maximum current density and located perpendicular to the magnetic field vectors in these points. Thin lines show magnetic field lines, bold lines are lines of equal current density.

rays, this mechanism is considered at the front of a shock wave propagating before plasma ejection. The occurrence of flares accompanied by fast ejections with powerful shock waves that did not cause solar cosmic rays (for example, flares on March 17 and 18, 2003), proves that solar cosmic rays are accelerated in the current sheet, and not on shock waves. This is due to the lack of a sufficient number of inhomogeneities near the shock wave from which particles could be reflected so that their effective acceleration occurs. Indeed, the Larmor radius of a proton with the energy of ~2 GeV in the magnetic field of the solar wind of $\sim 5 \times 10^{-4}$ Gs is $\sim 10^{10}$ cm; it corresponds to the dimension of the plasma inhomogeneity from which a particle could be reflected. The cluster of these huge heterogeneities in the solar wind has never been observed.

Measurements of cosmic-ray fluxes and thermal X-ray emission, whose peaks indicate the times of flare occurrence (data from the *GOES* spacecraft http://www.solarmonitor.org/index.php?date), show that for flares near the western edge of the solar disk, accelerated protons come with a delay of 15–20 min, which corresponds to the flight time from the western part of the disk along the magnetic line in the form of the Archimedes spiral. The rise time of the particle flux front from western flares is 15–30 min [32]. The delay time for the arrival of accelerated particles from flares that occurred on the eastern part of the solar

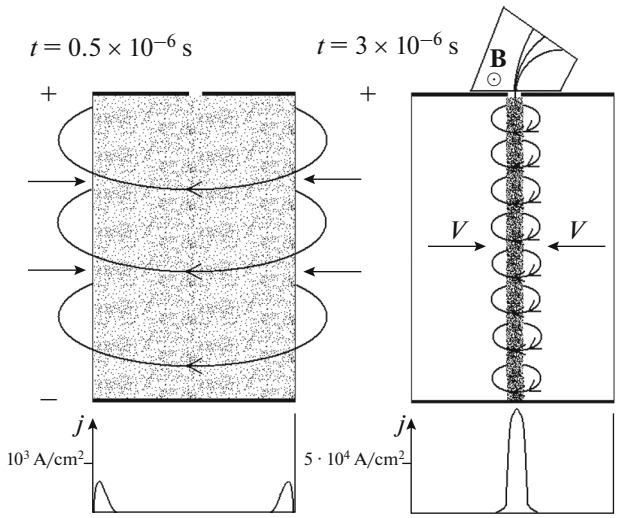

Fig. 9. Laboratory experiment with a powerful pulsed discharge demonstrating particle acceleration during compression of the discharge by its own magnetic field. The distribution of the discharge current density is at the bottom. Times $t = 0.5 \times 10^{-6}$ and $t = 3 \times 10^{-6}$ s are shown. The current increased with rate $dI/dt = 10^{11}$ A/s and reached a maximum value of 200 kA. At plasma compression rate $V \sim 10^7$ cm/s and magnetic field $B \sim 4 \times 10^4$ Gs, the electric field $\mathbf{E} = -\mathbf{V} \times \mathbf{B}/c$ equal to $E \sim 4 \times 10^3$ V/cm appears, which accelerates charged particles.

disk is 3–5 h, which is explained by the absence of the magnetic line connecting the place of the flare with the spacecraft in Earth's orbit, which is why direct passage of particles from the place of acceleration to the place of detection is impossible. Particles from eastern flares can reach the spacecraft moving across the magnetic field together with the solar wind (drift in crossed magnetic and electric fields). However, in this case, the delay in particle arrival would be ~3 days (the time of motion between the Sun and Earth with the velocity of the solar wind), which is much more than the observed delay of particle arrival. The observed delay can be explained by the diffusion of accelerated particles across the magnetic field due to their scattering on plasma inhomogeneities resulting from beam instability caused by the flux of accelerated particles along the field line [33]. The rise time of the particle flux front from eastern flares is ~1 day.

The time of existence of the solar cosmic-ray flux caused by the flare (usually ~3 days, sometimes reaches 10 days [27]) is more than two orders of magnitude longer than the time of the flare process, which is estimated by the time of thermal X-ray emission of the flare. Some protons that do not pass the entire distance along the field line to an observer propagate in a diffusion manner in interplanetary space for several days scattering on plasma inhomogeneities. During scattering, the spectrum of accelerated protons varies and this part of protons, called the slow component, is recorded by a network of neutron monitors already with the power-law spectrum [27, 30, 31]. The slow component of solar cosmic rays consists of particles propagating diffusely across the magnetic field, therefore, in contrast to the fast component, it appears not only from western, but also from eastern flares.

When using the fastest modern supercomputers, the planned MHD simulation above the active region and the simulation of the motion of test particles in the fields found above the active region are supposed to be used to forecast the occurrence of flares and solar cosmic-ray fluxes. Since there is no information on

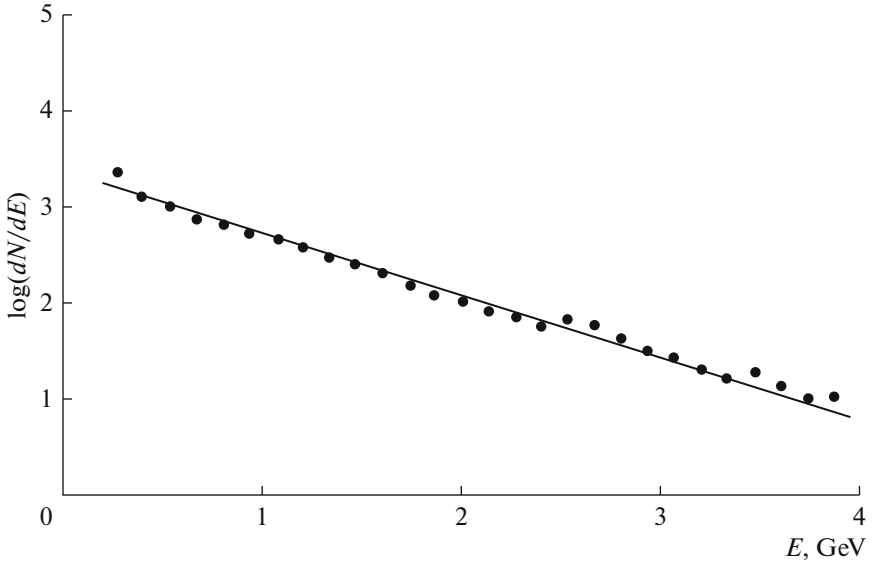

Fig. 10. The calculated spectrum of relativistic protons accelerated in the current sheet at the velocity of inflow into the sheet of 10^7 cm/s (points), and the spectrum measured on the network of neutron monitors.

plasma inhomogeneities, and, therefore, the diffusion coefficient in the equation of propagation of accelerated particles is unknown, it is assumed that the forecast of the propagation of cosmic rays in interplanetary space that can cause irradiation of cosmonauts is based on the performed analysis of observational data.

The pulses of relativistic protons accompanying some flares are detected against the background of the continuous flux of cosmic rays with an energy of more than 10^{15} eV. Their acceleration occurs outside the solar system. For more than 100 years, the acceleration of cosmic rays has been studied, but the physical mechanisms of acceleration remain unclear. The most popular, but not proven, hypothesis is the acceleration of protons in interstellar shock waves. However, there is no reason to believe that the mechanisms of particle acceleration on the Sun and other stars have a different nature. On the other hand, the energy of galactic cosmic rays is several orders of magnitude higher than the maximum energy of protons accelerated on the Sun. For a long time, this fact did not allow us to unequivocally state that the acceleration of stellar and solar cosmic rays occurs by the same mechanism. The discovery of giant flares on dwarf stars of the class G [34, 35] with energies significantly exceeding the energy of a solar flare indicates the possibility of acceleration of protons outside the solar system to energies significantly higher than the energy of solar cosmic rays. The results in [34, 35] can be considered as a new independent argument in favor of the generation of cosmic rays in flares rather than in shock waves. The occurrence of "superflares" with energies much higher observed during large solar flares was detected by the *Kepler* spacecraft for various G-class dwarf stars. Some of the dwarfs generating powerful flares rotate rapidly, and some with a rotation velocity on the order of the Sun [34]. This paper reports on 365 superflares on stars rotating with an angular velocity lower than the angular velocity of the Sun. In total, 83000 stars were studied with the *Kepler* spacecraft for 120 days. The previously considered significant difference in the maximum energies of galactic and solar cosmic rays did not contribute to the idea of their identical origin mechanisms, however, the discovery of superflares made the hypothesis of cosmic-ray acceleration more thorough. The data in [35] showed that the energy of a stellar flare can exceed 10^{35} erg, i.e., the energy of a large solar flare by 3–4 orders of magnitude, and, apparently, the energy of protons accelerated in these stellar flares can significantly exceed the energy of particles recorded from flares on the Sun. Thus, a flare can be a universal astronomical process responsible for the acceleration of protons on the Sun and on stars.

CONCLUSIONS

(1) The invariability of the magnetic field in the photosphere, shown for more than ten flares of several active regions, proves the appearance of a flare in the corona.

(2) Observations of UV emission in the lines of highly ionized iron ions that appear at temperatures considerably above the corona temperature give independent confirmation of the appearance of a flare in the corona.

(3) The appearance of a luminous structure several dozens of hours before the flare in the 94 Å Fe XVIII, which emits at the temperature of 6.3 MK (above the corona temperature of ~1 MK, but below the temperature at the flare location of 30–50 MK) can be used to predict solar flares.

(4) The coincidence of the position of the current sheet in the magnetic field obtained by MHD simulation in the corona above the active region with the position of the flare source of thermal X-ray emission is an independent proof of the mechanism of the solar flare, according to which the energy accumulated in the magnetic field of the current sheet is released.

(5) In the current sheet formed in the complex field of the solar corona, the physical meaning of the processes of accumulation and rapid release of flare energy is presented mainly not by magnetic lines of force, but lines in the configuration plane of the current sheet, tangent to the projections of the magnetic field vectors onto this plane.

(6) Based on the results of MHD simulation and observations, an electrodynamic model of a solar flare is proposed, explaining its main observational manifestations.

(7) The methods of MHD simulation in the corona above the active region in real time, necessary for more accurate study of the flare situation in the corona, have been prepared.

(8) Solar cosmic rays are accelerated by the electric field in the current sheet during the main flare process. The discovery of "superflares" on G-class dwarf stars, whose energy is 3–4 orders of magnitude higher than the energy of flares on the Sun, indicates the possibility of the identical mechanism for generating galactic and solar cosmic rays.

This performed study of the physical processes that occur during solar flares can help improve the forecast of the appearance of flares and solar cosmic rays.

REFERENCES

1. Lin, R.P., Krucker, S., Hurford, G.J., et al., RHESSI observations of particles acceleration and energy release in an intense gamma-ray line flare, *Astrophys. J.*, 2003, vol. 595, no.2, id L69.
2. Syrovatskii, S.I., Dynamic dissipation of magnetic energy in the vicinity of a neutral magnetic field line, *J. Exp. Theor. Phys.*, 1966, vol. 23, no. 4, pp. 754–762.
3. Podgorny, I.M. and Podgorny, A.I., MHD simulations of current-sheet formation over a bipolar active region, *Astron. Rep.*, 2003, vol. 47, no. 8, pp. 694–700.

4. Podgorny, A.I. and Podgorny, I.M., Magnetohydrodynamic simulation of a solar flare: 1. Current sheet in the corona, *Geomagn. Aeron. (Engl. Transl.)*, 2012, vol. 52, no. 2, pp. 150–161.
5. Forbes, T.G., Magnetic reconnection in solar flares, *Geophys. Astrophys. Fluid Dyn.*, 1991, vol. 62, no. 1, pp. 15–36.
6. Török, T. and Kliem, B., Confined and ejective eruptions of kink-unstable flux ropes, *Astrophys. J.*, 2005, vol. 630, no.1, pp. L97–L100.
7. Aulanier, G., Török, T., Démoulin, P., and DeLuca, E.E., Formation of torus-unstable flux ropes and electric currents in erupting sigmoids, *Astrophys. J.*, 2010, vol. 708, no. 1, pp. 314–333.
8. Zuccarello, F. P., Aulanier, G., Dudík, J., et al., Vortex and sink flows in eruptive flares as a model for coronal implosions, *Astrophys. J.*, 2017, vol. 837, no. 2, id 115.
9. Jiang, C., Wu, S.T., Yurchyshyn, V., et al., How did a major confined flare occur in super solar active region 12192?, *Astrophys. J.*, 2016, vol. 828, no. 1, id 62.
10. Podgorny, A.I. and Podgorny, I.M., Magnetic flux in an active solar region and its correlation with flares, *Astron. Rep.*, 2011, vol. 55, no. 7, pp. 629–636.
11. Podgorny, A.I. and Podgorny, I.M., Magnetic field distribution in the flare productive active region NOAA 10720, *J. Atmos. Sol. Terr. Phys.*, 2013, vol. 92, pp. 59–64.
12. Podgorny, A.I., Podgorny, I.M., and Meshalkina, N.S., Dynamics of magnetic fields of active regions in preflare states and during solar flares, *Astron. Rep.*, 2015, vol. 59, no. 8, pp. 795–805.
13. Podgorny, I.M. and Podgorny, A.I., UV radiation in the diagnostics of the development of the pre-flare state of solar corona and solar flare, *Proc. 40th Annual Apatity Seminar*, Apatity, 2017.
14. Podgorny, I.M. and Podgorny, A.I., Solar flares dynamics investigation using UV diagnostics, *Sun Geosphere*, 2018, vol. 13, no. 1, pp. 69–76.
15. Podgorny, A.I. and Podgorny, I.M., Magnetohydrodynamic simulation of a solar flare: 2. Flare model and simulation using active-region magnetic maps, *Geomagn. Aeron. (Engl. Transl.)*, 2012, vol. 52, no. 2, pp. 162–175.
16. Podgorny, A.I. and Podgorny, I.M., MHD simulation of solar flare current sheet position and comparison with X-ray observations in active region NOAA 10365, *Sun Geosphere*, 2013, vol. 8, no. 2, pp. 71–76.
17. Podgorny, I.M., Simulation studies of space, *Fundam. Cosmic Phys.*, 1978, vol. 4, no. 1, pp. 1–72.
18. Podgorny, A.I. and Podgorny, I.M., Formation of several current sheets preceding a series of flares above the active region AR 0365, *Astron. Rep.*, 2008, vol. 85, no. 8, pp. 666–675.
19. Podgorny, A.I. and Podgorny, I.M., MHD modeling of phenomena in the solar corona using an absolutely implicit scheme, *Comput. Math. Math. Phys.*, 2004, vol. 44, no. 10, pp. 1784–1806.
20. Podgorny, A.I. and Podgorny, I.M., Positions of X-ray emission sources of solar flare obtained by MHD simulation, *Physics of Auroral Phenomena: Proc. of the 36th Annual Seminar*, Apatity: Kola Science Center, 2013, pp. 117–120.
21. Podgorny, A.I. and Podgorny, I.M., A model of a solar flare: Comparisons with observations of high-energy processes, *Astron. Rep.*, 2006, vol. 50, no. 10, pp. 842–850.
22. Hiei, E. and Hundhausen, A.J., Development of a coronal helmet streamer of 24 January 1992, *Magnetodynamic Phenomena in the Solar Atmosphere*, Uchida, Y., Kosugi, T., and Hudson, S., Eds., Kluwer, 1996, pp. 125–126.
23. Masuda, S., Kosugi, T., Hara, H., et al., A loop-top hard X-ray source in a compact solar flare as evidence for magnetic reconnection, *Nature*, 1994, vol. 371, no. 6497, pp. 495–497.
24. Krucker, S., Wuelser, J.-P., Vourlidas, A., et al., STEREO and RHESSI observations of electron acceleration in a partially Disk-Occulted Solar Flare, *Proc. of the 12th European Solar Physics Meeting (ESPM-12), Freiburg, Germany*, 2008, p. 2.84.
25. Borisenko, A.V., Podgorny, I.M., and Podgorny, A.I., The use of supercomputers in studying the solar flare mechanism by MHD-simulation in the corona, *Solnechno–zemnaya fizika: sovremennoe sostoyanie i perspektiva. Konferentsiya "Astronomiya-2018"* (Solar–Terrestrial Physics: State of the Art and Prospects. Conference "Astronomya-2018"), Moscow, GAISh MGU, 2018, p. 39.
26. Podgorny, A.I. and Podgorny, I.M., Particle acceleration in the current sheath, *Izv. Ross. Acad. Nauk: Ser. Phys.*, 1997, vol. 61, no. 6, pp. 1067–1069.
27. Podgorny, I.M. and Podgorny, A.I., Solar cosmic ray acceleration and propagation, *Sun Geosphere*, 2016, vol. 11, no. 2, pp. 85–90.
28. Luk'yanov, S.Yu. and Podgorny, I.M., Hard X-ray radiation accompanying a discharge in gas, *At. Energ.*, 1956, vol. 1, no. 3, pp. 97–106.
29. Podgorny, I.M., Koval'skii, N.G., and Pal'schikov, V.E., Electrons causing hard X-ray radiation of pulse discharges, *Dokl. Akad. Nauk*, 1958, vol. 123, pp. 825–827.
30. Podgorny, I.M., Balabin, Yu.V., Vashenyuk, E.V., et al., The generation of hard X-rays and relativistic protons observed during solar flares, *Astron. Rep.*, 2010, vol. 54, no. 7, pp. 645–656.
31. Podgorny, I.M., Balabin, Yu.V., Podgorny, A.I., et al., Spectrum of solar flare protons, *J. Atmos. Sol. Terr. Phys.*, 2010, vol. 72, no. 13, pp. 988–991.
32. Podgorny, I.M. and Podgorny, A.I., Proton acceleration in the solar flare, *J. Atmos. Sol. Terr. Phys.*, 2018, vol. 180, pp. 9–15.
33. Istomin, Ya.N., Relativistic jets in active galactic nuclei: time variability, *Mon. Not. R. Astron. Soc.*, 2010, vol. 408, no. 2, pp. 1307–1312.
34. Maehara, H., Shibayama, T., Notsu, S., et al., Superflares on solar-type stars, *Nature*, 2012, vol. 485, no. 7399, pp. 478–481.
35. Shibayama, T., Maehara, H., Notsu, S., et al., Superflares on solar-type stars observed with *Kepler*. I. Statistical properties of superflares, *Astrophys. J. Suppl.*, 2013, vol. 209, no. 1, id 5.

Translated by N. Topchiev